TU Delft

Delft University of Technology

Probing the Jaynes-Cummings Ladder with Spin Circuit Quantum Electrodynamics

Bonsen, Tobias; Harvey-Collard, Patrick; Russ, Maximilian; Dijkema, Jurgen; Sammak, Amir; Scappucci, Giordano; Vandersypen, Lieven M.K.

DOI
10.1103/PhysRevLett.130.137001

Publication date
2023

Document Version
Final published version

Published in
Physical review letters

Citation (APA)
Bonsen, T., Harvey-Collard, P., Russ, M., Dijkema, J., Sammak, A., Scappucci, G., & Vandersypen, L. M. K. (2023). Probing the Jaynes-Cummings Ladder with Spin Circuit Quantum Electrodynamics. *Physical review letters*, *130*(13), Article 137001. https://doi.org/10.1103/PhysRevLett.130.137001

Important note
To cite this publication, please use the final published version (if applicable).
Please check the document version above.

Copyright
Other than for strictly personal use, it is not permitted to download, forward or distribute the text or part of it, without the consent of the author(s) and/or copyright holder(s), unless the work is under an open content license such as Creative Commons.

Takedown policy
Please contact us and provide details if you believe this document breaches copyrights.
We will remove access to the work immediately and investigate your claim.

This work is downloaded from Delft University of Technology.
For technical reasons the number of authors shown on this cover page is limited to a maximum of 10.

Probing the Jaynes-Cummings Ladder with Spin Circuit Quantum Electrodynamics

Tobias Bonsen,[1] Patrick Harvey-Collard,[1] Maximilian Russ,[1] Jurgen Dijkema,[1] Amir Sammak,[2] Giordano Scappucci,[1] and Lieven M. K. Vandersypen[1,*]

[1]*QuTech and Kavli Institute of Nanoscience, Delft University of Technology, 2628 CJ Delft, Netherlands*
[2]*QuTech and Netherlands Organization for Applied Scientific Research (TNO), 2628 CJ Delft, Netherlands*

(Received 25 April 2022; accepted 11 January 2023; published 27 March 2023)

We report observations of transitions between excited states in the Jaynes-Cummings ladder of circuit quantum electrodynamics with electron spins (spin circuit QED). We show that unexplained features in recent experimental work correspond to such transitions and present an input-output framework that includes these effects. In new experiments, we first reproduce previous observations and then reveal both excited-state transitions and multiphoton transitions by increasing the probe power and using two-tone spectroscopy. This ability to probe the Jaynes-Cummings ladder is enabled by improvements in the coupling-to-decoherence ratio, and shows an increase in the maturity of spin circuit QED as an interesting platform for studying quantum phenomena.

DOI: 10.1103/PhysRevLett.130.137001

Spin qubits in gate-defined silicon quantum dots (QDs) are a promising platform for quantum computing thanks to their small footprint, excellent coherence properties, and compatibility with today's highly advanced semiconductor industry [1–4]. Circuit quantum electrodynamics with spins, or spin circuit QED for short, focuses on the coherent coupling of spin qubits to photons in high-quality-factor superconducting resonators. This can be used to achieve long-range two-qubit gates and readout of the qubit state [5], paving the way to a scalable architecture for quantum computing based on spins in linked quantum-dot arrays [6]. Following advances of circuit QED with superconducting qubits [7–9], spin circuit QED has been achieved in several device architectures by leveraging spin-charge hybridization to couple the electron spin to the resonator electric field [10–13]. Experiments with single electron spins in silicon [14,15] and multispin qubits in gallium arsenide [16] have achieved spin-photon coupling strengths that exceed the resonator and qubit linewidths, thereby reaching the strong coupling regime. Subsequently, simultaneous resonant interaction between a resonator and two spins has been achieved [17], followed by resonator-mediated interaction between two remote spins in the dispersive regime [18]. Additionally, spin circuit QED has been employed to achieve spin-transmon coupling [19] and single-shot gate-based readout of spin qubits [20]. The present Letter is motivated by results from the strong spin-photon coupling experiment of Samkharadze *et al.* [14]. In this experiment, spin-charge hybridization was achieved by engineering an artificial spin-orbit interaction in a Si/SiGe double quantum dot (DQD). The resulting spin-photon coupling was characterized with a spectroscopic measurement of the resonator transmission. Specifically, the transmission as a function of probe frequency and magnetic field strength, reproduced here in Fig. 1(a), shows a vacuum Rabi splitting of the modes, signaling the coherent hybridization of the spin with a single microwave photon. An additional feature appears in the gap near the lower branch (arrow), which has remained unexplained until now. Additional peaks in a spectrum generally hint at the involvement of additional transitions in the system, which can spoil the behavior of resonator-mediated interactions. The development of a scalable spin-circuit-QED architecture will therefore require a deeper understanding of this phenomenon.

In this Letter, we explain the physical origin of the observed feature. We first find that its frequency matches transitions between excited states in the Jaynes-Cummings ladder. Analogous signatures have also been observed in earlier circuit QED experiments with superconducting transmon qubits [28,29]; however, in the spin-photon system they exhibit a different characteristic shape due to specific differences, and had not been identified as such. We then develop a theoretical framework that combines input-output theory [21,30,31] with a Lindblad master equation [32,33]. This theory captures transitions between excited states in the Jaynes-Cummings ladder, probe-power-dependent effects, and two-tone spectroscopy. The simulated spectra reproduce well the observed feature in the vacuum Rabi splitting. We show data from new experiments in which we both reproduce the observations of Samkharadze *et al.* [14] and furthermore reveal new multiphoton transitions [34]. We demonstrate the capability to drive some of these transitions, which could be useful for future photon preparation and detection schemes [35,36].

The first step to explain the presence of the additional feature in the spectrum in Fig. 1(a) is to identify the transitions involved. To this end, we compare the data to the

 © 2023 American Physical Society

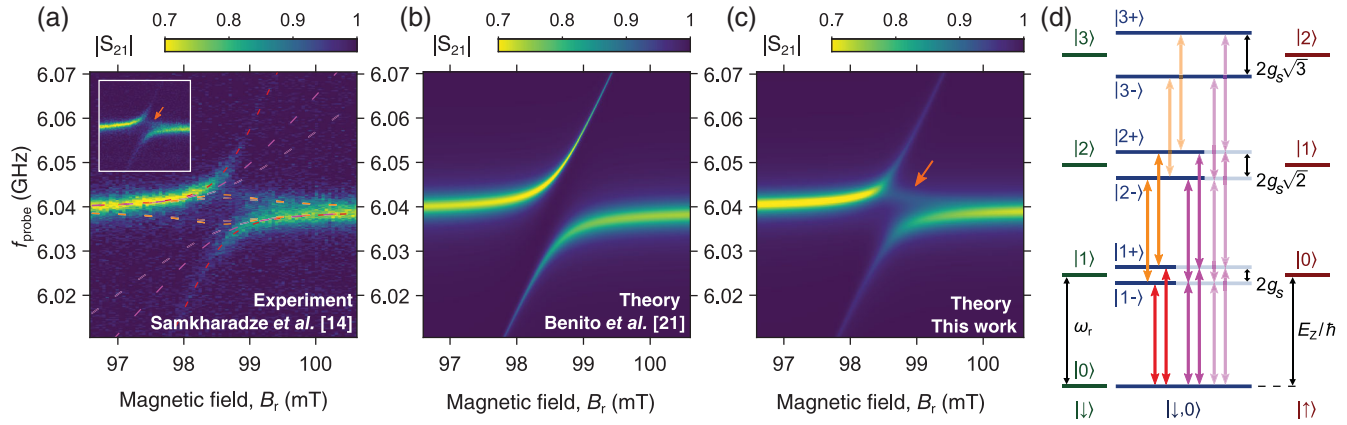

FIG. 1. (a) Experimental resonator transmission spectrum from Samkharadze *et al.* [14] for $2t_c/h = 10.4$ GHz, together with transition frequencies (dashed lines) in the Jaynes-Cummings ladder in (d). Inset: the data is replotted without transition frequencies overlay. The avoided crossing demonstrates strong spin-photon coupling. An additional, previously unexplained feature appears inside the vacuum Rabi split peaks (arrow). (b) Transmission spectrum predicted by the standard input-output theory for spin circuit QED [21] using the parameters in Supplemental Table S1 [22]. (c) Simulated spectrum using the theory presented in this Letter for probe amplitude $a_{\mathrm{in},1} = 1000\ \mathrm{Hz}^{1/2}$, thermal bath temperature $T = 200$ mK, and other parameters in Supplemental Table S1 [22]. Since this experiment uses a hanger-style resonator, resulting in a resonance dip, the color scale has been inverted to match the transmission-style resonator data presented later in this Letter. (d) Transitions in the resonant spin-photon Jaynes-Cummings ladder: main branches of the avoided crossing (red), excited-state transitions (orange) that correspond to the observed additional feature within the gap in (a), and multiphoton transitions (purple).

transition frequencies calculated from the system Hamiltonian $H = H_0 + H_r + H_I$, see Fig. 2. The full details of the spin-photon interaction have been described elsewhere [5,12,37]. The Hamiltonian for the double quantum dot containing one electron is given by

$$H_0 = \frac{1}{2}(\epsilon\tau_z + 2t_c\tau_x + g_e\mu_B B_z\sigma_z + g_e\mu_B B_x\sigma_x\tau_z), \quad (1)$$

where τ_α and σ_α are the Pauli operators for position (left, right) and spin $(\uparrow,\downarrow)$, respectively, $g_e = 2$ is the Landé g factor in silicon, and μ_B is the Bohr magneton. At zero charge detuning, i.e., when $\epsilon = 0$ μeV, the electron charge eigenstates with energy splitting $2t_c$ ("charge qubit") develop a significant charge dipole that enables charge-photon and spin-photon interaction. This interaction can be

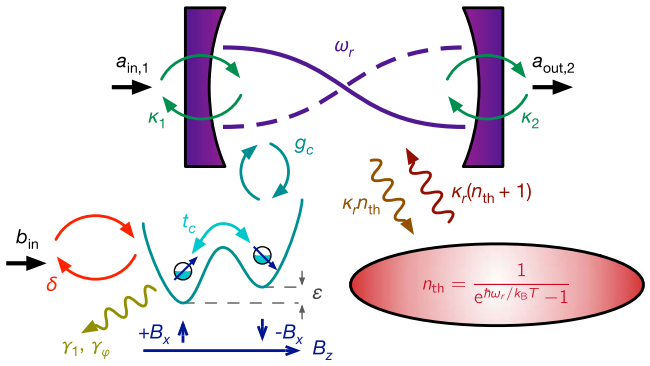

FIG. 2. Overview of the input-output model for the coupled DQD-resonator system (see main text).

turned off by localizing the electron onto a single dot, i.e., $|\epsilon| \gg |t_c|$. The applied external magnetic field (with magnitude B_r in the experiments), together with micromagnets fabricated on top of the DQD gate structure, result in a magnetic field gradient at the location of the DQD. The homogeneous magnetic field component B_z induces most of the Zeeman splitting of the electron spin states and is related to B_r using the micromagnet model in Supplemental Material Sec. S1 B, while the interdot magnetic field difference $2B_x$ causes spin and orbital states to hybridize [22,37]. The resonator is modeled as a single-mode harmonic oscillator with Hamiltonian $H_r = \hbar\omega_r a^\dagger a$, and directly couples to the DQD charge degree of freedom via its detuning. This interaction can be described as $H_I = \hbar g_c(a^\dagger + a)\tau_z$, with g_c the charge-photon coupling strength. In the eigenbasis of H_0 this interaction acquires off-diagonal elements, which facilitates a spin-photon coupling $g_s \le g_c$ mediated by the charge states of the DQD [22]. Near spin-photon resonance, the eigenenergies of the system form the Jaynes-Cummings ladder depicted in Fig. 1(d) [22,38].

In the experiment, transitions between the system eigenstates are probed by measuring the transmission of a weak probe signal at frequency $f_{\mathrm{probe}} = \omega_{\mathrm{probe}}/2\pi$. This coherent probe is described by a time-dependent driving term

$$V(t) = i\hbar\sqrt{\kappa_1}(e^{-i\omega_{\mathrm{probe}}t}a_{\mathrm{in},1}a^\dagger - e^{i\omega_{\mathrm{probe}}t}a^*_{\mathrm{in},1}a), \quad (2)$$

where κ_1 is the coupling strength between the resonator and the probe signal of coherent amplitude $a_{\mathrm{in},1}$. The probe

power is related to this amplitude through $P_{\text{probe}} = \lambda\hbar\omega_{\text{probe}}|a_{\text{in},1}|^2$, where λ accounts for extra losses in the probe signal delivery line [39]. For the two-tone simulations presented later in this Letter, a similar driving term $W(t)$ is added to describe a DQD pump tone with coherent amplitude b_{in} [22].

Having described the system and its Hamiltonian, we now examine different classes of transitions that could match the spectrum in Fig. 1(a). The vacuum-Rabi-split modes correspond to the $|\downarrow, 0\rangle \leftrightarrow |1\pm\rangle$ transitions (red) in the Jaynes-Cummings ladder [Fig. 1(d)]. We find that the observed additional feature in the upper part of the gap closely matches the frequency of the $|1+\rangle \leftrightarrow |2+\rangle$ transition in the ladder, while the $|1-\rangle \leftrightarrow |2-\rangle$ transition frequency lies in the lower part of the gap, where no additional features are visible in the Samkharadze *et al.* [14] experiment [Fig. 1(a)]. Together, these transition frequencies (orange) form an eyelike shape in the middle of the gap. Transitions involving higher states in the ladder, i.e., $|m\pm\rangle \leftrightarrow |(m+1)\pm\rangle$ for $m \geq 2$ (transparent orange), move progressively closer to the middle of the spectrum for higher m. Eventually they converge to a straight crossing of the modes that corresponds to the classical limit [29]. Circuit QED experiments with transmon qubits have reported observations of features corresponding to these excited-state transitions [28], as well as features corresponding to multiphoton transitions from the ground state to higher excited states in the ladder [34]. These multiphoton transitions form a fanlike structure in the spectrum (purple) and are not observed in the data from Samkharadze *et al.* [14]. Later in this Letter, we present new experiments with a different device that confirm the transition labeling.

To understand the relative visibility of these transitions, we now turn to an input-output description of the system. We first find the steady-state density matrix of the driven system from the Lindblad master equation

$$\frac{d\rho}{dt} = -\frac{i}{\hbar}[H + V(t), \rho] + \gamma_1 \mathcal{D}[\tilde{\tau}_-](\rho) + \frac{\gamma_\phi}{2}\mathcal{D}[\tilde{\tau}_z](\rho) + (n_{\text{th}} + 1)\kappa_r \mathcal{D}[a](\rho) + n_{\text{th}}\kappa_r \mathcal{D}[a^\dagger](\rho), \tag{3}$$

with Lindblad dissipator $\mathcal{D}[A](\rho) = A\rho A^\dagger - \frac{1}{2}\{A^\dagger A, \rho\}$. Charge relaxation (rate γ_1) and charge dephasing (rate γ_ϕ) are described with Pauli operators $\tilde{\tau}_-$ and $\tilde{\tau}_z$ in the hybridized eigenbasis of charge states $|\pm\rangle$ [21,32]. The resonator linewidth $\kappa_r = \kappa_1 + \kappa_2 + \kappa_{\text{int}}$ consists of losses from coupling to the input-output lines ($\kappa_1 = \kappa_2$) and internal losses (κ_{int}). Figure 2 gives an overview of this model. Spin decoherence due to nuclear spins in ^{28}Si is much weaker than the decoherence caused by charge noise that couples in through spin-charge hybridization [14,15], and is therefore not included in this Letter.

The appearance of the feature inside the vacuum Rabi splitting requires a sufficient population of the excited states in the ladder, specifically the $|1+\rangle$ state. For probe frequencies within the gap, excitation to these states by the coherent probe signal is suppressed, but could be caused by several other mechanisms. Here, we empirically model incoherent excitations by coupling the resonator to a boson bath at temperature T with a thermal occupation $n_{\text{th}} = 1/[\exp(\hbar\omega_r/k_B T) - 1]$ [29]. For $g_c = 0$, this will result in a thermal resonator state with temperature T, while for $g_c \neq 0$, this will lead to a finite population of excited DQD-resonator states. However, other mechanisms, like charge or spin excitation (or thermalization) effects can also populate the $|1+\rangle$ state, and can therefore produce similar signatures in the spectrum. These mechanisms could not be differentiated here (see Supplemental Material Sec. S3 for an example of a thermal spin model [22]).

To find the steady state of the system, we first apply a multilevel rotating wave approximation (RWA) to get a time-independent master equation. We then truncate the resonator Hilbert space and transform all operators into the Liouville space [33,40,41], to arrive at a matrix-vector equation that can be numerically solved to find the steady-state density operator ρ_S [22]. The resonator transmission is then given by

$$S_{21} = \frac{a_{\text{out},2}}{a_{\text{in},1}} = \frac{\langle\sqrt{\kappa_2}a\rangle}{a_{\text{in},1}} = \frac{\sqrt{\kappa_2}\,\text{Tr}(a\rho_S)}{a_{\text{in},1}}. \tag{4}$$

The results from the experiment by Samkharadze *et al.* [14] are well reproduced by simulations using this theoretical framework, as shown in Fig. 1(c). To obtain good agreement, we first determine the Hamiltonian parameters by matching the calculated Jaynes-Cummings transition frequencies to the experimental data. We then manually adjust the bath temperature T, the probe amplitude $a_{\text{in},1}$, and the charge decoherence rates γ_1, γ_ϕ to match the relative visibility of transitions in the spectrum. The reason to proceed like this is mainly that the model has a large number of parameters that are underconstrained when fit to a single spectrum. Obtaining an automated fit would require simultaneously fitting to multiple heterogeneous datasets. Alternatively, independent measurements can be used to determine certain parameters (more details in Supplemental Material Sec. S1 H [22]). At $T = 200$ mK, a finite population of excited Jaynes-Cummings states makes higher transitions in the ladder (orange) visible in the spectrum. In this case, this leads to the appearance of a feature inside the vacuum Rabi splitting, which corresponds predominantly to the $|1+\rangle \leftrightarrow |2+\rangle$ transition. Furthermore, the finite probe signal amplitude $a_{\text{in},1} = 1000\ \text{Hz}^{1/2}$ makes the main branches appear less bright near the top and bottom of the spectrum compared to the standard input-output simulation [Fig. 1(b)]. This broadening of the spinlike transitions away from spin-photon resonance is also observed in the experiment [Fig. 1(a)] and results from the finite population of higher-photon-number states generated by the probe signal. Specifically, the simulated average photon number

reaches $\langle a^\dagger a\rangle = \mathrm{Tr}(a^\dagger a\rho_S) = 0.31$ for $B_r = 99$ mT, which effectively broadens the spinlike transitions due to photon-number-dependent dispersive shifts [18]. Increasing $a_{\mathrm{in},1}$ further in the simulations leads to a reduced vacuum Rabi splitting and the appearance of multiphoton transitions [34] in the spectrum. However, these effects are not observed in the results from Samkharadze *et al.* [14], since the probe power was kept low in their experiment. Finally, the charge decoherence rates γ_1, γ_ϕ make transitions in the lower part of the spectrum (involving $|m-\rangle$ states) more or less visible compared to features in the upper part (involving $|m+\rangle$ states) depending on their strength. This effect is also observed in the experiment [Fig. 1(a)] and simulations using the standard input-output theory [Fig. 1(b)]. It is caused by an asymmetric admixture with the charge degree of freedom (i.e., the photonlike transition has less charge component below spin-photon resonance than above spin-photon resonance). To match the relative visibility of upper and lower features in the experimental data, the simulations [Figs. 1(b) and 1(c)] use charge decoherence rates $\gamma_1/2\pi = 20$ MHz and $\gamma_\phi/2\pi = 200$ MHz.

We now describe a new set of experiments in which we intentionally probe the transitions of the Jaynes-Cummings ladder described above. The device, experimental setup, and data acquisition are described in detail in Ref. [18] and were designed to realize resonator-mediated spin-spin interactions. Here, we only use one of the DQDs (DQD2 in the nomenclature of Ref. [18]), allowing its spin to interact with the resonator photons, while the other remains decoupled. This system achieves a charge-photon coupling strength of $g_c/2\pi = 192$ MHz and is operated at a DQD tunnel coupling of $2t_c/h = 12.0$ GHz for these experiments, resulting in an effective spin-photon coupling strength of $g_s/2\pi \approx 16$ MHz. Since the bare resonator linewidth is $\kappa_r/2\pi = 2.5$ MHz and the spin linewidth is $\gamma_s/2\pi \leq 6$ MHz, the strong spin-photon coupling regime is achieved. For a weak probe signal, the measured transmission spectrum in Fig. 3(a) shows a simple avoided crossing of the main modes, while additional features are hardly visible. The small dent in the upper branch around $B_r = 53.2$ mT is believed to be an accidental crossing with a defect (two-level system). When the probe power is increased, see Fig. 3(b), features corresponding to both the $|m+\rangle \leftrightarrow |(m+1)+\rangle$ and $|m-\rangle \leftrightarrow |(m+1)-\rangle$ transitions become visible to form an eyelike shape in the spectrum (orange lines). Additionally, a faint feature appears near the upper branch that corresponds to the $|\downarrow, 0\rangle \leftrightarrow |2+\rangle$ transition involving two-photon processes (purple line) [34].

These results are well predicted by simulations using the theory developed for this work and shown in Figs. 3(c) and 3(d). To obtain good agreement, we employ the same manual fitting procedure as before and vary both the probe amplitude $a_{\mathrm{in},1}$ and the bath temperature T between the low-power [Fig. 3(c)] and high-power [Fig. 3(d)] simulations. The increase in $a_{\mathrm{in},1}$ leads to a fading of the

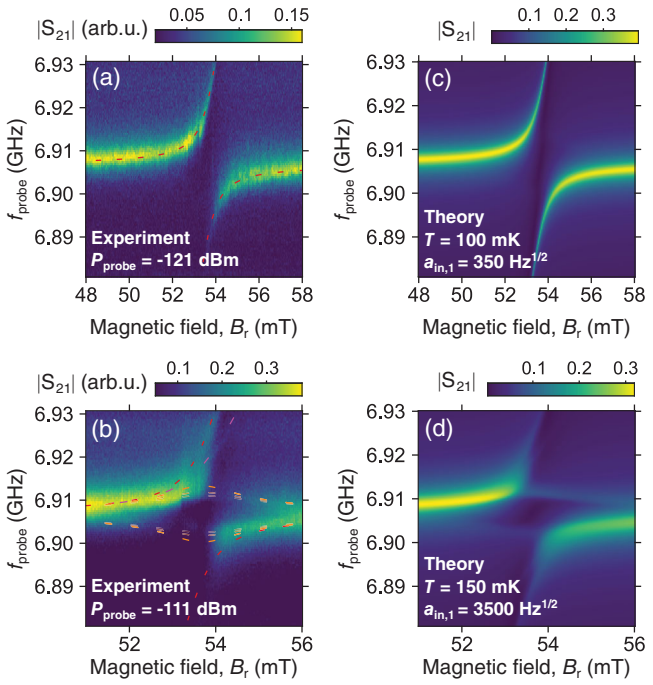

FIG. 3. (a),(b) Resonator transmission spectra taken using the new device from Ref. [18] at low (a,c) and high (b,d) probe power probe power with relevant transition frequencies in the Jaynes-Cummings ladder, see Fig. 1(d). Here, "low" and "high" probe power refers to the simulated average photon numbers $\langle a^\dagger a\rangle < 0.1$ and $\langle a^\dagger a\rangle > 1$ that are reached away from spin-photon resonance. (c),(d) Simulated spectra using the theory presented in this Letter and the parameters in Supplemental Table S1 [22].

branches near the top and the bottom of the spectrum, a reduced vacuum Rabi splitting, and the appearance of the $|\downarrow, 0\rangle \leftrightarrow |2+\rangle$ transition in the simulated spectrum. Interestingly, the high-power simulation uses an increased T compared to the low-power simulation. This increase in T is needed to get agreement in the visibility of the eyelike feature, and might suggest a connection between the probe power and the effective temperature of the system.

Next, we reveal the eyelike transitions (orange) using a pump tone [see Fig. 4(a)] to generate population of the excited states [28]. This pump tone increases the steady-state occupation of the $|1\pm\rangle$ states, such that features corresponding to the $|1\pm\rangle \leftrightarrow |2\pm\rangle$ transitions become more apparent. The measured spectrum in Fig. 4(b) indeed reveals a feature corresponding to the $|1+\rangle \leftrightarrow |2+\rangle$ transition, while the feature corresponding to the $|1-\rangle \leftrightarrow |2-\rangle$ transition remains faint. Using this pump-plus-weak-probe scheme, the extra Jaynes-Cummings transition appears in a more targeted way than in the previous strong-probe scheme of Figs. 3(b) and 3(d).

To model this two-tone experiment, a second driving term $W(t)$ that couples to the DQD detuning is added to the master equation in Eq. (3). Since the Hamiltonian then contains terms rotating at two different frequencies, the RWA fails to eliminate the time dependence in the master

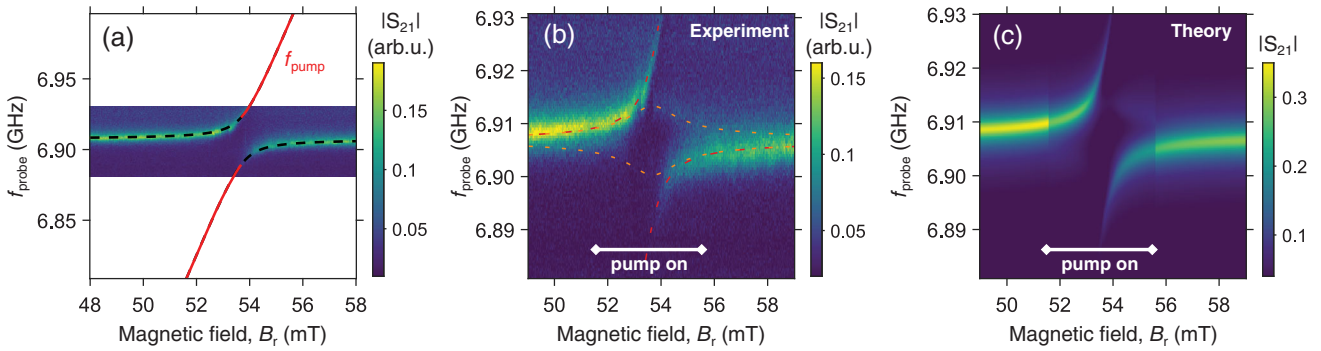

FIG. 4. Two-tone spectroscopy scheme. (a) The $|\downarrow,0\rangle \leftrightarrow |1\pm\rangle$ transition frequencies are fitted to the spectrum at low probe power. The frequency of the additional pump tone (red line) is set to the $|\downarrow,0\rangle \leftrightarrow |1-\rangle$ transition (lower branch) for magnetic fields $51.60\ \text{mT} \leq B_r \leq 53.65\ \text{mT}$ and to the $|\downarrow,0\rangle \leftrightarrow |1+\rangle$ transition (upper branch) for $53.65\ \text{mT} < B_r \leq 55.60\ \text{mT}$. (b) Measured transmission spectrum with transition frequencies in the Jaynes-Cummings ladder, see Fig. 1(d). (c) Simulated spectrum using the two-tone input-output model in Supplemental Material Sec. S1 G [22] for thermal bath temperature $T = 200$ mK, pure charge dephasing rate $\gamma_\phi/2\pi = 120$ MHz, and other parameters in Supplemental Table S1 [22].

equation and we can no longer find a steady-state solution as before. To circumvent this issue, we assume the probe signal is weak and calculate the resonator transmission in the linear response regime [22]. The simulated spectrum using this approach in Fig. 4(c) shows good qualitative agreement with the measured data. The sharp changes of visibility in the simulated spectrum appear due to the switching on and off of the pump tone, and are also observed in the experiment to some degree.

In summary, we have observed additional transitions in the vacuum Rabi splitting spectrum of spin circuit QED devices. We have identified these transitions as involving higher excited states in the Jaynes-Cummings ladder, thereby also explaining previously reported observations. The visibility of these transitions was enhanced by increasing the probe power and by using a pump-and-probe scheme. We found the experimental data to be in agreement with simulations using an input-output framework based on a steady-state solution of a Lindblad master equation. Improvements in the coupling-to-decoherence ratio (cooperativity) enable more distinct observations of these transitions, allowing one to probe higher transitions in the Jaynes-Cummings ladder. In that regard, the new experiments presented here are a witness of the improvements in cooperativity in this spin-photon system. In the future, selective driving of these transitions could prove useful for photon preparation and measurement schemes [35,36]. Finally, the input-output framework presented in this Letter can be straightforwardly extended to accurately describe resonator-mediated interactions between two spins, which pave the way to a scalable spin qubit architecture [6,17,18].

The data and simulation scripts used in this Letter are archived online [42].

The authors thank G. Zheng for his contributions to setting up the experiment, L. P. Kouwenhoven and his team for access to the NbTiN film deposition, F. Alanis Carrasco for assistance with sample fabrication, and other members of the spin qubit team at QuTech for useful discussions. This research was undertaken thanks in part to funding from the European Research Council (ERC Synergy Quantum Computer Lab), and the Dutch Ministry for Economic Affairs through the allowance for Topconsortia for Knowledge and Innovation (TKI).

P. H.-C. and T. B. identified the relevant transitions from the Hamiltonian model. T. B. and M. R. developed the theoretical framework. P. H.-C., J. D., and T. B. performed the electrical cryogenic measurements. P. H.-C. fabricated the device. A. S. contributed to sample fabrication. A. S. grew the heterostructure with G. S.'s supervision. T. B., P. H.-C., J. D., M. R., and L. M. K. V. analyzed the results. T. B. wrote the manuscript with input from all co-authors. P. H.-C. and L. M. K. V. supervised the project.

*Corresponding author.
L.M.K.Vandersypen@tudelft.nl

[1] D. Loss and D. P. DiVincenzo, Quantum computation with quantum dots, Phys. Rev. A **57**, 120 (1998).
[2] R. Hanson, L. P. Kouwenhoven, J. R. Petta, S. Tarucha, and L. M. K. Vandersypen, Spins in few-electron quantum dots, Rev. Mod. Phys. **79**, 1217 (2007).
[3] F. A. Zwanenburg, A. S. Dzurak, A. Morello, M. Y. Simmons, L. C. L. Hollenberg, G. Klimeck, S. Rogge, S. N. Coppersmith, and M. A. Eriksson, Silicon quantum electronics, Rev. Mod. Phys. **85**, 961 (2013).
[4] A. M. J. Zwerver *et al.*, Qubits made by advanced semiconductor manufacturing, Nat. Electron. **5**, 184 (2022).
[5] G. Burkard, M. J. Gullans, X. Mi, and J. R. Petta, Superconductor–semiconductor hybrid-circuit quantum electrodynamics, Nat. Rev. Phys. **2**, 129 (2020).
[6] L. M. K. Vandersypen, H. Bluhm, J. S. Clarke, A. S. Dzurak, R. Ishihara, A. Morello, D. J. Reilly, L. R. Schreiber, and M. Veldhorst, Interfacing spin qubits in

quantum dots and donors—hot, dense, and coherent, npj Quantum Inf. **3**, 34 (2017).
[7] A. Blais, R.-S. Huang, A. Wallraff, S. M. Girvin, and R. J. Schoelkopf, Cavity quantum electrodynamics for superconducting electrical circuits: An architecture for quantum computation, Phys. Rev. A **69**, 062320 (2004).
[8] A. Wallraff, D. I. Schuster, A. Blais, L. Frunzio, R.-S. Huang, J. Majer, S. Kumar, S. M. Girvin, and R. J. Schoelkopf, Strong coupling of a single photon to a superconducting qubit using circuit quantum electrodynamics, Nature (London) **431**, 162 (2004).
[9] A. Blais, S. M. Girvin, and W. D. Oliver, Quantum information processing and quantum optics with circuit quantum electrodynamics, Nat. Phys. **16**, 247 (2020).
[10] M. Trif, V. N. Golovach, and D. Loss, Spin dynamics in InAs nanowire quantum dots coupled to a transmission line, Phys. Rev. B **77**, 045434 (2008).
[11] A. Cottet and T. Kontos, Spin Quantum Bit with Ferromagnetic Contacts for Circuit QED, Phys. Rev. Lett. **105**, 160502 (2010).
[12] X. Hu, Y.-x. Liu, and F. Nori, Strong coupling of a spin qubit to a superconducting stripline cavity, Phys. Rev. B **86**, 035314 (2012).
[13] V. Srinivasa, J. M. Taylor, and C. Tahan, Entangling distant resonant exchange qubits via circuit quantum electrodynamics, Phys. Rev. B **94**, 205421 (2016).
[14] N. Samkharadze, G. Zheng, N. Kalhor, D. Brousse, A. Sammak, U. C. Mendes, A. Blais, G. Scappucci, and L. M. K. Vandersypen, Strong spin-photon coupling in silicon, Science **359**, 1123 (2018).
[15] X. Mi, M. Benito, S. Putz, D. M. Zajac, J. M. Taylor, G. Burkard, and J. R. Petta, A coherent spin–photon interface in silicon, Nature (London) **555**, 599 (2018).
[16] A. J. Landig, J. V. Koski, P. Scarlino, U. C. Mendes, A. Blais, C. Reichl, W. Wegscheider, A. Wallraff, K. Ensslin, and T. Ihn, Coherent spin–photon coupling using a resonant exchange qubit, Nature (London) **560**, 179 (2018).
[17] F. Borjans, X. G. Croot, X. Mi, M. J. Gullans, and J. R. Petta, Resonant microwave-mediated interactions between distant electron spins, Nature (London) **577**, 195 (2020).
[18] P. Harvey-Collard, J. Dijkema, G. Zheng, A. Sammak, G. Scappucci, and L. M. K. Vandersypen, Coherent Spin-Spin Coupling Mediated by Virtual Microwave Photons, Phys. Rev. X **12**, 021026 (2022).
[19] A. J. Landig, J. V. Koski, P. Scarlino, C. Müller, J. C. Abadillo-Uriel, B. Kratochwil, C. Reichl, W. Wegscheider, S. N. Coppersmith, M. Friesen, A. Wallraff, T. Ihn, and K. Ensslin, Virtual-photon-mediated spin-qubit–transmon coupling, Nat. Commun. **10**, 5037 (2019).
[20] G. Zheng, N. Samkharadze, M. L. Noordam, N. Kalhor, D. Brousse, A. Sammak, G. Scappucci, and L. M. K. Vandersypen, Rapid gate-based spin read-out in silicon using an on-chip resonator, Nat. Nanotechnol. **14**, 742 (2019).
[21] M. Benito, X. Mi, J. M. Taylor, J. R. Petta, and G. Burkard, Input-output theory for spin-photon coupling in *Si* double quantum dots, Phys. Rev. B **96**, 235434 (2017).
[22] See Supplemental Material at http://link.aps.org/supplemental/10.1103/PhysRevLett.130.137001 for details on the input-output framework, simulation parameters, extended data, and additional references [23–27].
[23] D. Zeuch, F. Hassler, J. J. Slim, and D. P. DiVincenzo, Exact rotating wave approximation, Ann. Phys. (Amsterdam) **423**, 168327 (2020).
[24] P. Harvey-Collard, G. Zheng, J. Dijkema, N. Samkharadze, A. Sammak, G. Scappucci, and L. M. K. Vandersypen, On-Chip Microwave Filters for High-Impedance Resonators with Gate-Defined Quantum Dots, Phys. Rev. Appl. **14**, 034025 (2020).
[25] L. S. Bishop, Circuit quantum electrodynamics, Ph.D. thesis, Yale University, 2010.
[26] X. Croot, X. Mi, S. Putz, M. Benito, F. Borjans, G. Burkard, and J. R. Petta, Flopping-mode electric dipole spin resonance, Phys. Rev. Res. **2**, 012006(R) (2020).
[27] M. Benito, X. Croot, C. Adelsberger, S. Putz, X. Mi, J. R. Petta, and G. Burkard, Electric-field control and noise protection of the flopping-mode spin qubit, Phys. Rev. B **100**, 125430 (2019).
[28] J. Fink, M. Göppl, M. Baur, R. Bianchetti, P. J. Leek, A. Blais, and A. Wallraff, Climbing the Jaynes–Cummings ladder and observing its nonlinearity in a cavity QED system, Nature (London) **454**, 315 (2008).
[29] J. M. Fink, L. Steffen, P. Studer, L. S. Bishop, M. Baur, R. Bianchetti, D. Bozyigit, C. Lang, S. Filipp, P. J. Leek, and A. Wallraff, Quantum-to-Classical Transition in Cavity Quantum Electrodynamics, Phys. Rev. Lett. **105**, 163601 (2010).
[30] M. Benito and G. Burkard, Hybrid superconductor-semiconductor systems for quantum technology, Appl. Phys. Lett. **116**, 190502 (2020).
[31] S. Kohler, Dispersive readout: Universal theory beyond the rotating-wave approximation, Phys. Rev. A **98**, 023849 (2018).
[32] M. Benito, J. R. Petta, and G. Burkard, Optimized cavity-mediated dispersive two-qubit gates between spin qubits, Phys. Rev. B **100**, 081412(R) (2019).
[33] D. Manzano, A short introduction to the Lindblad master equation, AIP Adv. **10**, 025106 (2020).
[34] L. S. Bishop, J. M. Chow, J. Koch, A. A. Houck, M. H. Devoret, E. Thuneberg, S. M. Girvin, and R. J. Schoelkopf, Nonlinear response of the vacuum Rabi resonance, Nat. Phys. **5**, 105 (2009).
[35] B. R. Johnson, M. D. Reed, A. A. Houck, D. I. Schuster, L. S. Bishop, E. Ginossar, J. M. Gambetta, L. DiCarlo, L. Frunzio, S. M. Girvin, and R. J. Schoelkopf, Quantum non-demolition detection of single microwave photons in a circuit, Nat. Phys. **6**, 663 (2010).
[36] V. V. Albert, K. Noh, K. Duivenvoorden, D. J. Young, R. T. Brierley, P. Reinhold, C. Vuillot, L. Li, C. Shen, S. M. Girvin, B. M. Terhal, and L. Jiang, Performance and structure of single-mode bosonic codes, Phys. Rev. A **97**, 032346 (2018).
[37] F. Beaudoin, D. Lachance-Quirion, W. A. Coish, and M. Pioro-Ladrière, Coupling a single electron spin to a microwave resonator: Controlling transverse and longitudinal couplings, Nanotechnology **27**, 464003 (2016).
[38] E. T. Jaynes and F. W. Cummings, Comparison of quantum and semiclassical radiation theories with application to the beam maser, Proc. IEEE **51**, 89 (1963).
[39] J. Gambetta, A. Blais, D. I. Schuster, A. Wallraff, L. Frunzio, J. Majer, M. H. Devoret, S. M. Girvin, and R. J. Schoelkopf, Qubit-photon interactions in a cavity:

Measurement-induced dephasing and number splitting, Phys. Rev. A **74**, 042318 (2006).

[40] A. A. Dzhioev and D. S. Kosov, Super-fermion representation of quantum kinetic equations for the electron transport problem, J. Chem. Phys. **134**, 044121 (2011).

[41] U. Harbola and S. Mukamel, Superoperator nonequilibrium Green's function theory of many-body systems; applications to charge transfer and transport in open junctions, Phys. Rep. **465**, 191 (2008).

[42] https://dx.doi.org/10.4121/19336748.